
Generating Adversarial Fragments with Adversarial Networks for Physical-world Implementation

Zelun Kong and Cong Liu

Department of Computer Science

Erik Jonsson School of Engineering & Computer Science

The University of Texas at Dallas

{zelun.kong, cong}@utdallas.edu

Abstract

Although deep neural networks have been widely applied in many application domains, they are found to be vulnerable to adversarial attacks. A recent promising set of attacking techniques have been proposed, which mainly focus on generating adversarial examples under digital-world settings. Such strategies are unfortunately not implementable for any physical-world scenarios such as autonomous driving. In this paper, we present FragGAN, a new GAN-based framework which is capable of generating an adversarial image which differs from the original input image only through replacing a targeted fragment within the image using a corresponding visually indistinguishable adversarial fragment. FragGAN ensures that the resulting entire image is effective in attacking. For any physical-world implementation, an attacker could physically print out the adversarial fragment and then paste it onto the original fragment (e.g., a roadside sign for autonomous driving scenarios). FragGAN also enables clean-label attacks against image classification, as the resulting attacks may succeed even without modifying any essential content of an image. Extensive experiments including physical-world case studies on state-of-the-art autonomous steering and image classification models demonstrate that FragGAN is highly effective and superior to simple extensions of existing approaches. To the best of our knowledge, FragGAN is the first approach that can implement effective and clean-label physical-world attacks.

1 Introduction

Deep neural networks (DNNs) have achieved tremendous success in many application domains such as autonomous driving and image classification Hinton et al. (2012); He et al. (2017). However, recent studies show that, even though a well-trained neural network generalizes well on the test set, it may still be vulnerable to adversarial attacks Goodfellow et al. (2014b); Eykholt et al. (2018a); Lin et al. (2017); Carlini and Wagner (2017); Li and Vorobeychik (2015, 2014); Kos et al. (2018). Through adding small-magnitude perturbations to an instance, the resulting adversarial example could mislead DNNs with a high success rate. Different approaches have been proposed for producing adversarial examples, including the earliest work revealing the existence of such examples Szegedy et al. (2013), and various optimization-based methods (e.g., the fast gradient sign method (FGSM) Goodfellow et al. (2014b)) that are shown to be effective under various scenarios Carlini and Wagner (2017); Moosavi-Dezfooli et al. (2016); Liu et al. (2016); Xiao et al. (2018b); Eykholt et al. (2017). Recently, Xiao et al. (2018a) presents a technique leveraging generative adversarial network (GAN) on the conditional adversarial network to produce adversarial examples which may achieve high semi-blackbox attack success rate.

Unfortunately, existing techniques on generating adversarial examples mostly focus on digital-world attacking and are inapplicable to realistic scenarios imposing physical-world constraints, such as

autonomous driving. One technique developed on generating physical-world adversarial example is recently presented in Eykholt et al. (2018a). The proposed technique is highly interesting (first of its kind) and effective to its focused scene. However, the applicability is rather limited as the technique requires to manually stick the generated perturbations (e.g., white and black stickers) onto the stop sign, which fails the important clean-label attack goal (i.e., human labelers shall not be able to recognize that the stop sign gets modified in any noticeable manner). Another key technical limitation is that the process of generating the perturbation has not considered any potential background imagery commonly associated with the stop sign in the physical world (e.g., the sky or the road). This prevents the technique to be implemented in realistic scenarios such as autonomous driving, since the attacking efficacy may dramatically decrease (even ineffective at all) as the image captured by any car dash camera will contain such background imagery besides the stop sign.

For any adversarial attacking technique to be effective in physical-world scenarios, a key challenge (also a key difference from digital-world scenarios) is the following: only particular fragments of an input image could be physically modified for adversarial purposes. For instance, consider autonomous driving, it is simply impossible to implement an adversarial example in practice which adds perturbations to the sky. Such attacks may work in digital-world yet not implementable in physical-world. Thus, attacking techniques have to be able to generate adversarial examples through modifying only particular fragments (e.g., roadside signs within any car dash camera-captured image frame) instead of the entire image, while still ensuring the resulting image containing the generated adversarial fragments to be effective in attacking.

Motivated by these observations, in this paper, we present FragGAN, a GAN-based framework that is capable of producing arbitrary (w.r.t. size and position) adversarial fragments within an input image which can be applied in physical-world scenarios such as autonomous driving, resolving the key challenge mentioned earlier. Specifically, given an input image and the four coordinates of the targeted quadrilateral fragment in the image, FragGAN is able to output an adversarial image which differs from the original image only by replacing the targeted fragment with a generated adversarial fragment visually indistinguishable from the original one. FragGAN ensures that the resulting entire adversarial image is effective in attacking. For physical-world implementation, an attacker could print out the adversarial fragment and paste it onto the original object (e.g., a roadside sign).

To achieve this goal, FragGAN develops a new GAN-based architecture which differs from the existing adversarial GAN-based ones (e.g., AdvGAN Xiao et al. (2018a) and AC-GAN Song et al. (2018)). In particular, FragGAN introduces an encoder component, which is the convolutional neural network (CNN) part of the trained target network to pre-process the original image instance and extract the features. Doing so enables FragGAN to generate an adversarial fragment considering the remaining image info other than the targeted fragment. This is actually key to guarantee the attacking efficacy of the generated adversarial example. Without this encoder, the efficacy would dramatically decrease since the test-time prediction depends on the entire image but not the fragment itself. Another unique feature is that FragGAN is capable of directly generating adversarial fragments without any human intervention. This is fundamentally different from traditional GAN-based attacking techniques (e.g., Xiao et al. (2018a)), which first generate perturbation and then add it to the original image with a human-set co-efficient controlling perturbation intensity. Furthermore, our design of FragGAN enables both white-box attacks and distilled attacks (i.e., the semi-blackbox attacks defined in Xiao et al. (2018a)) which do not require to directly access the model parameters and structure.

We prove the effectiveness and robustness of FragGAN by conducting extensive experiments using various state-of-the-art autonomous steering models and driving-specific datasets. Results show that FragGAN is rather effective for various steering models and scenes, yielding an average steering angle error up to 23 degrees. We have also conducted physical-world case studies, which apply FragGAN to generate adversarial fragments corresponding to two commonly seen roadside signs, and then print out and paste the generated fragment physically onto the original roadside sign on campus. Results prove the effectiveness of FragGAN when being applied to real-world driving scenarios, where a steering angle error of 13.2 and 19.8 degree is achieved for the two scenes, respectively. We also highlight a key novelty of our design by comparing FragGAN against a new baseline approach we develop, which straightforwardly combines AdvGAN Xiao et al. (2018a) with the idea of generating adversarial fragments. This comparison reveals a key technical advantage of FragGAN, that FragGAN generates adversarial fragments with the purpose of making the resulting entire adversarial image to be effective in attacking. Any straightforward extension of existing techniques would not be effective

because the entire background imagery is not considered during the process of generating adversarial fragments.

Besides application to physical-world attacks, we also demonstrate in evaluation that FragGAN may enable practical, clean-label attacks to the general image classification domain. Being able to generate arbitrary adversarial fragments within an input image allows an attacker to completely avoid modifying the content essential to the task (which can be decided by the attacker). With FragGAN, an attacker can generate adversarial fragments only corresponding to those non-essential content belonging to the image while being effective in attacking. This would more likely enable a clean-label adversarial example as the essential content of an input image (which actually defines the label according to human labelers) is completely unmodified.

2 Related Work

Adversarial Examples. A number of recent techniques have been proposed to generate adversarial examples Szegedy et al. (2013); Goodfellow et al. (2014b); Xiao et al. (2018b); Hu and Tan (2017). The fast gradient sign method (FGSM) Goodfellow et al. (2014b) represents the first of such methods, which performs an one-step gradient update along the direction of the sign of gradient at each pixel. OTCM Kurakin et al. (2016) extended FGSM to a targeted attack strategy by maximizing the probability of the target class. Several optimization-based methods Tanay and Griffin (2016); Liu et al. (2016); Carlini and Wagner (2017); Xiao et al. (2018a) have also been proposed to craft adversarial examples via optimization. These methods all focus on adding perturbations to the entire image in a digital-world setting and do not consider physical-world constraints. Another recent work Karmon et al. (2018) proposes to generate perturbations that are confined to a small, localized patch of the image. However, there are a couple of major drawbacks associated with this approach. First, the generated perturbation is too obvious, for any human labeler, which actually directly contradicts with the essential benefit and motivation behind confining perturbations to a small area of the image (i.e., generating clean-label attacks without modifying the essential content of the image). Second, this technique targets at digital-world attacking scenarios, thus being inapplicable to physical-world implementation. It suffers a similar yet fundamental drawback as Eykholt et al. (2017), where the algorithm for generating perturbations does not integrate the entire background imagery into consideration, which may cause the resulting entire image to lose attack efficacy. Both these drawbacks are resolved in our design of FragGAN.

Physical-world attacks. A very recent set of works took the first step in studying physical-world attacking of static physical objects Athalye et al. (2017); Metzen et al. (2017), human objects Sharif et al. (2016); Elsayed et al. (2018), stop sign Sermanet and LeCun (2011); Mogelmose et al. (2012), and roadside sign Zhou et al. (2018). Although these works prove to be effective under the targeted scenarios and certain assumptions, they mostly focus on studying a static physical-world scene (e.g., a single snapshot of a stop sign Eykholt et al. (2018b); Sermanet and LeCun (2011)), and their generated adversarial samples are visually unrealistic (e.g., a billboard painted by various bright colors which are too obvious for attack purposes Zhou et al. (2018)). Moreover, as discussed earlier, a key technical limitation is that the process of generating the perturbation has not considered any potential background imagery commonly associated with the targeted object (e.g., a stop sign in Eykholt et al. (2018b) and a billboard in Zhou et al. (2018)) in the physical world (e.g., the sky or the road). This prevents the technique to be implemented in realistic scenarios such as autonomous driving, since the attacking efficacy may dramatically decrease (even ineffective at all) as the image captured by any car dash camera will contain such background imagery besides the stop sign.

GAN-based Methods. GAN was first introduced in Goodfellow et al. (2014a), implemented by a system of two neural networks contesting with each other in a zero-sum game framework. GAN is proved to be able to achieve visually appealing results in both face generation Lu et al. (2017) and manipulation Zhu et al. (2016). In order to further improve the quality of synthesis images, image-to-image GAN has been proposed such as the conditional GAN Isola et al. (2017) and the CycleGAN Zhu et al. (2017), which learn a loss function to train the mapping from the input image to the output image. Xiao et al. (2018a) presents AdvGAN, which leverages GAN to produce adversarial samples with high success rate. Different from these GAN-based approaches, FragGAN focuses on generating a physically implementable adversarial image in which only those arbitrarily selected fragments in the original image are replaced using the generated adversarial fragments.

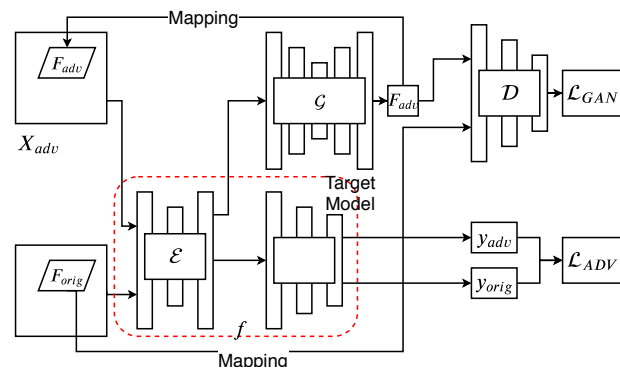


Figure 1: Overview of the FragGAN framework.

3 Generating Adversarial Fragments

Problem Definition. Let \mathcal{X} be the feature space with n number of features, $\mathcal{X} \subseteq \mathbb{R}^n$. Let \mathcal{Y} be the real value set for regression or the class set for classification. Suppose (X_i, y_i) is the i^{th} sample in the dataset, which is composed of feature vector $X_i \in \mathcal{X}$ and $y_i \in \mathcal{Y}$, the corresponding real value or true class label. X_i subjects to some unknown distribution $X_i \sim \mathcal{P}_{data}$. The learning system aims to learn a model $f: \mathcal{X} \rightarrow \mathcal{Y}$ from the feature space \mathcal{X} to the target set \mathcal{Y} .

Given an instance (X_i, y_i) , the goal of FragGAN is to produce an adversarial sample X_{adv} , which aims to mislead the target neural network f as $f(X_i) \neq y_i$. To achieve the goal, FragGAN will generate an adversarial fragment F_{adv} , which is a fragment of X_i , and use it to substitute original fragment F_{orig} , which is the corresponding part of X_i originally, and finally output an adversarial sample X_{adv} . The adversarial fragment F_{adv} is supposed to be close to the original fragment F_{orig} in terms of $L2$ or other distance metrics, which implies that adversarial fragment F_{adv} and original fragment F_{orig} are visually indistinguishable for human labelers.

The FragGAN Framework. Fig. 1 illustrates the overall architecture of FragGAN, which mainly consists of four components: an encoder \mathcal{E} , a generator \mathcal{G} , a discriminator \mathcal{D} and the target neural network f . The encoder \mathcal{E} is a convolutional neural network, which is used to extract features of a sample (of both adversarial and original ones). The extracted features of original sample X_{orig} will be used as the inputs fed to the generator to generate an adversarial fragment F_{adv} . Doing so allows FragGAN to take into account the fact that different original sample X_{orig} may have different influence on the generated adversarial fragment F_{adv} , thus ensuring the generator \mathcal{G} to generate the best adversarial fragment F_{adv} corresponding to a specific original sample X_{orig} . Note that GAN-generated images are normally of square shape. Since performing a perspective mapping will only output a quadrilateral out of a square, thus adversarial fragment F_{adv} and original fragment F_{orig} are required to be quadrilaterals. The adversarial fragment F_{adv} and original fragment F_{orig} will then be sent to the discriminator \mathcal{D} , which is used to distinguish the adversarial fragment F_{adv} and the original fragment F_{orig} . The discriminator \mathcal{D} can intuitively be viewed as a loss function, which measures the visual distinction between adversarial fragment F_{adv} and original fragment F_{orig} , and then encourages the generator to generate visually indistinguishable fragments compared to the original ones.

To encourage the adversarial fragment F_{adv} generated by the generator \mathcal{G} to be close to the original fragment F_{orig} , we jointly train the generator \mathcal{G} and discriminator \mathcal{D} . The discriminator \mathcal{D} and generator \mathcal{G} form an adversarial learning scheme by optimizing the opposite object. The generative adversarial loss \mathcal{L}_{GAN} Goodfellow et al. (2014a) can be written as:

$$\mathcal{L}_{GAN} = \mathbb{E}_{F_{orig} \sim p_{F_{orig}}} \log \mathcal{D}(F_{orig}) + \mathbb{E}_{F_{adv} \sim p_{F_{adv}}} \log(1 - \mathcal{D}(F_{adv})) \quad (1)$$

After obtaining the generated adversarial fragment F_{adv} , we use it to produce an adversarial sample X_{adv} by using it to replace the corresponding fragment originally presented in the image. A challenge herein is that the generated adversarial fragment F_{adv} is a square image and the original fragment could be an arbitrary quadrilateral area. We thus leverage a classical perspective mapping method per (2019) to resolve this mismatch, as illustrated in Fig. 2.

As seen in the figure, the quadrilateral $(O, r_{10}, r_{11}, r_{01})$ is the original area of the original fragment F_{orig} that is chosen to be substi-

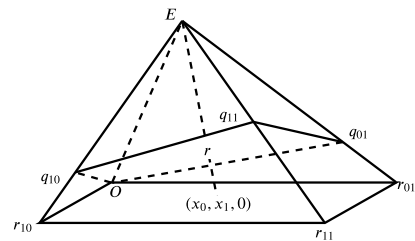


Figure 2: Perspective mapping.

tuted, and the square $(O, q_{10}, q_{11}, q_{01})$ represents the generated adversarial fragment F_{adv} . Since each pixel r in the area $(O, r_{10}, r_{11}, r_{01})$ will have one or more corresponding pixels in the area $(O, q_{10}, q_{11}, q_{01})$, the final RGB value of r can be calculated using existing 2-dimension interpolation methods int (2019) such as the nearest neighbor interpolation, bilinear interpolation, or bicubic interpolation.

The fractional linear transformation that maps the square to the quadrilateral is given by per (2019):

$$(y_0, y_1) = \frac{(a_0 x_0, a_1 x_1)}{(a_0 + a_1 - 1) + (1 - a_1)x_0 + (1 - a_0)x_1}, \quad (2)$$

where (y_0, y_1) is subject to

$$\overrightarrow{Or} = y_0 \overrightarrow{Or_{10}} + y_1 \overrightarrow{Or_{01}} \quad (3)$$

The fractional linear transformation that maps the quadrilateral to the square is:

$$(x_0, x_1) = \frac{(a_1(a_0 + a_1 - 1)y_0, a_0(a_0 + a_1 - 1)y_1)}{a_0a_1 + a_1(a_1 - 1)y_0 + a_0(a_0 - 1)y_1}, \quad (4)$$

where the coefficients a_0 and a_1 are constructed as the solution of two linear equations in two unknowns:

$$\overrightarrow{Or_{11}} = a_0 \overrightarrow{Or_{10}} + a_1 \overrightarrow{Or_{01}} \quad (5)$$

In order to fulfill the goal of misleading the target neural network f by an adversarial sample X_{adv} , we first train the generator \mathcal{G} jointly with the target neural network f . The target neural network f respectively takes the extracted features of original sample X_{orig} and adversarial sample X_{adv} as its inputs. Then, the two outputs of the target neural network $f(\mathcal{E}(X_{orig}))$ and $f(\mathcal{E}(X_{adv}))$ are used to calculate \mathcal{L}_{ADV}^f , which represents how much does the target neural network f is misled.

The loss for misleading the target neural network f in attack is:

$$\mathcal{L}_{ADV}^f = \beta \exp(-\frac{1}{\beta} \cdot l_f(f(X_{orig}), f(X_{adv}))), \quad (6)$$

where β is a sharpness parameter and l_f denotes the loss function used to train the target neural network f , such as MSE-loss or L1-loss for regression or cross-entropy loss for classification. By minimizing \mathcal{L}_{ADV}^f , the distance between the prediction and the ground truth will be maximized, which ensure the attacking effectiveness.

Finally, the ultimate objective of FragGAN can be expressed as:

$$\mathcal{L} = \mathcal{L}_{GAN} + \lambda \mathcal{L}_{ADV}^f, \quad (7)$$

where λ denotes a coefficient to balance the tradeoff between the two terms.

To interpret this objective function, \mathcal{L}_{GAN} encourages the adversarial fragment F_{adv} to appear visually similar to the original fragment F_{orig} , while \mathcal{L}_{ADV}^f is leveraged to generate adversarial sample X_{adv} which optimizes for high attack effectiveness. We obtain the generator \mathcal{G} , discriminator \mathcal{D} by solving:

$$\arg \min_{\mathcal{G}} \max_{\mathcal{D}} \mathcal{L}. \quad (8)$$

Once generator \mathcal{G} and discriminator \mathcal{D} are trained on the dataset and the target neural network f , adversarial fragment F_{adv} can be produced for any original sample X_{orig} as input to perform an attack.

White-box Attack. For generating white-box attack under FragGAN, we assume that the target neural network f was pre-trained and the parameters of target neural network f are fixed, and the generator \mathcal{G} of FragGAN can only access the parameters of the target neural network f during training. FragGAN performs the following steps in an iterative manner to generate white-box attacks:

1. **Update discriminator \mathcal{D} given the fixed encoder \mathcal{E} and generator \mathcal{G} :** In this step, generator \mathcal{G} takes the extracted features $\mathcal{E}(X_{orig})$ as its input and generates an adversarial

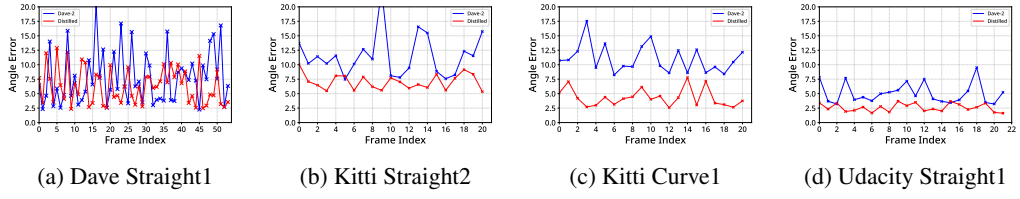


Figure 3: Results on the steering angle error.

fragment F_{adv} . Then, we will transform the original quadrilateral fragment area into a square fragment using the perspective mapping method and using the transformed square fragment to substitute the original fragment F_{orig} in the original sample X_{orig} . Finally, both original fragment F_{orig} and adversarial fragment F_{adv} will be used to train discriminator \mathcal{D} , encouraging the discriminator \mathcal{D} to distinguish them. The objective is (see Eq. (1)):

$$\arg \max_{\mathcal{D}} \mathcal{L}_{GAN}. \quad (9)$$

2. **Update generator \mathcal{G} given the fixed encoder \mathcal{E} and discriminator \mathcal{D} :** In this step, generator \mathcal{G} firstly takes the extracted feature $\mathcal{E}(X_{orig})$ as its input and generates an adversarial fragment F_{adv} . Then, the adversarial fragment F_{adv} , in the square shape, will be transformed into the original quadrilateral shape and embedded into the sample. The resulting sample will be the adversarial sample X_{adv} . Finally, adversarial sample X_{adv} and original sample X_{orig} will be respectively sent to target neural network f . The objective of this step is to learn a generator \mathcal{G} which minimize the \mathcal{L}_{ADV} (see (Eq. (6)):

$$\arg \min_{\mathcal{G}} (\mathcal{L}_{GAN} + \lambda \mathcal{L}_{ADV}^f). \quad (10)$$

Distilled Attack. For generating distilled attacks under FragGAN, we assume FragGAN cannot access the parameters of the target neural network f directly during training phase. To perform distilled attacks, FragGAN first builds a distilled neural network Hinton et al. (2015) d based on the target neural network f .

Once we have d distilled from the target neural network f through the knowledge distillation method, d will behave very similar to the target neural network f according to Hinton et al. (2015). Then, using d to substitute the target neural network position in FragGAN, we can carry out the same steps of performing white-box attacks mentioned earlier. The knowledge distillation objective is:

$$\arg \min_d \mathcal{H}(d(X_{orig}), f(X_{orig})), \quad (11)$$

where $d(X_{orig})$ and $f(X_{orig})$ denote the distilled neural network and the target neural network f (which is a black-box model herein), respectively, and \mathcal{H} denotes the commonly used cross-entropy loss in knowledge distillation.

4 Evaluation

In this section, we first evaluate FragGAN for both white-box and distilled attacks on state-of-the-art autonomous steering models and datasets. These experiments cover both digital evaluation and actual physical-world case studies. Then, we show the effectiveness of applying FragGAN for attacking image classification models.

4.1 Apply FragGAN to Attack State-of-the-art Autonomous Steering Models

Before presenting evaluation details, we note that due to space constraints, we only put a partial set of the experimental results in the paper (e.g., demonstrating the results focusing on the DAVE-2 steering model instead of all four evaluated models, as well as a randomly selected set of datasets and scenes). We put all additional evaluation results in an appendix uploaded as supplementary material.

Datasets, Steering Models, and Evaluation Metrics. For white-box attack, we use pre-trained Convolutional Neural Network originating from NVIDIA’s DAVE-2 System dav (2019a) and three other state-of-the-art DNN-driven autonomous steering models as the targeted steering models, which have been widely used in autonomous driving testing Ma et al. (2018); Pei et al. (2017); Tian et al. (2018); Zhang et al. (2018). For distilled attack, we distill each steering model to get a new corresponding model, denoted as DAVE2-Distilled for DAVE2 for instance. The datasets used in

	Dave		Udacity	Kitti		
	Straight1	Curve1	Straight1	Straight1	Curve1	Straight2
AdvGANFragGAN						
AdvGAN						
AdvGAN (Frag)						

Table 1: Comparison of AdvGAN, AdvGAN(fragment) and FragGAN on steering models. The blue (red, green and purple, respectively) arrow indicates the ground truth steering angle (the erroneous steering angle due to FragGAN, AdvGAN, and AdvGAN(frag), respectively).

our experiments include: (1) Udacity automatic driving car challenge dataset uda (2019) which contains 101396 training images captured by a dashboard-mounted camera of a driving car and the simultaneous steering wheel angle applied by a human driver for each image; (2) DAVE-2 testing dataset Pan et al. (2017); dav (2019b) which contains 45,568 images to test the NVIDIA DAVE-2 model; and (3) Kitti Geiger et al. (2013) dataset which contains 14,999 images from six different scenes captured by a VW Passat station wagon equipped with four video cameras. We evaluate the efficacy of the attacking by measuring the average steering angle error among all frames in each evaluated scene, which denotes steering angle divergence between the ground-truth steering angle and the misled steering angle under FragGAN.

Driving Scene Selection Criteria. Our driving scene selection criteria is that the roadside traffic or advertising boards should appear entirely in the first frame of a driving video with more than 400 pixels and partially disappear in the last frame. We select seven scenes from the aforementioned datasets and evaluate on all selected scenes. We present results on a partial set of scenes in the paper and include the rest in an appendix.

White-box Attack. For White-box attack, we train the generator in FragGAN using the originally trained target steering models, which is a convolutional neural network. The adversarial fragment generated by FragGAN will be mapped into every image according to the perspective mapping method to produce an adversarial example image. Then we use the target steering models to predict the adversarial images and compare them against the ground-truth steering decisions recorded in a given scene that we select according to the aforementioned criteria.

Distilled Attack. For distilled attack, we firstly train a distilled steering model from each evaluated steering model, using the knowledge distillation method, and then train the generator in FragGAN using each distilled model. After the adversarial fragments are generated, they are mapped into their corresponding frame to produce the adversarial examples. Finally, we use each of the four evaluated steering models to predict the steering angle through the adversarial images and compare them against the ground-truth steering angle recorded in a given scene.

Comparison against Existing Approaches. To highlight the efficacy and novelty of FragGAN, we have compared against other approaches including AdvGAN Xiao et al. (2018a), and AdvGAN(frag), a straightforward extension of AdvGAN integrating the idea of generating only adversarial fragments. AdvGAN(frag) applies AdvGAN to add perturbations only to the same fragments targeted by FragGAN. We note that comparing FragGAN directly against AdvGAN is actually unfair because, in practice, it is simply impossible to add perturbations to an entire image frame captured by an on-vehicle camera.

Results. The attacking effectiveness results in terms of the steering angle error along the timeline for four scenes are shown in Fig. 3, where the x-axis is the indexes of the image frame along the timeline, and the y-axis is the steering angle error. Note that for digital-world evaluations, we generate an adversarial fragment under each evaluated scene for each frame, as the four coordinates of the targeted fragment are different in different frames.

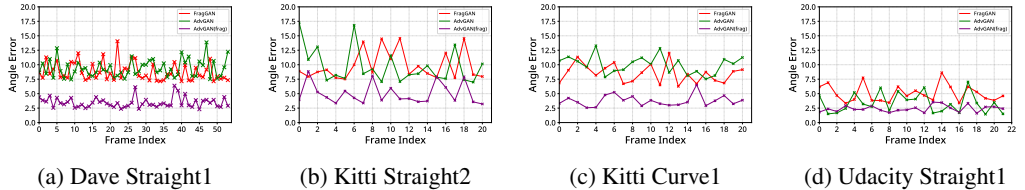


Figure 4: Comparison among FragGAN, AdvGAN, and AdvGAN(frag) on different datasets and the DAVE-2 model.

We observe that under both Dave-2 and the distilled Dave-2 models, FragGAN is able to cause a noticeable steering angle error under all scenes. For instance, for the *Kitti Straight2* scene, an average steering angle error of 12.5 and 6.1 degrees are achieved among all frames under the Dave-2 and the distilled model, respectively. Moreover, the maximum angle error is quite significant, ranging from 13–23 degrees and 5–12.5 degrees under the Dave-2 and the distilled model among all scenes, respectively. Such large angle errors could cause dangerous driving actions and accidents in practice. We also observe that the generator trained by the distilled model yields weaker performance, which is due to the typical knowledge loss due to the distilling process Hinton et al. (2015).

For the comparison with AdvGAN, sample results are shown in the second and third rows in the Table 1. The observation is that FragGAN yields similar (a few cases better) attacking effectiveness in terms of steering angle error compared to AdvGAN. This shows the strength of FragGAN as this evaluation (in an unfair manner) allows AdvGAN to modify the entire digital image. The first and third rows in Table 1 show the result of the comparison between FragGAN and AdvGAN(frag). AdvGAN(frag) yields a minimal degree of attacking efficacy as the steering angle under the adversarial scenario is almost identical to the ground truth steering angle; while FragGAN is able to mislead the steering model by a significant margin. As mentioned earlier, this highlights the technical novelty of FragGAN of developing a new GAN-based architecture which can generate adversarial fragments with the purpose of making the resulting entire adversarial image to be effective in attacking, through considering the entire background imagery during the process of generating adversarial fragments.

Physical-world Case Studies. We also perform a set of proof-of-concept physical-world case studies. We target the roadside sign commonly seen during driving as the fragment of our interest. We use FragGAN to generate two adversarial fragments corresponding to two common advertising signs for McDonald’s and Apple Watch, assuming a fixed distance between a car dash camera and the roadside sign. We then print out and paste each adversarial fragment onto the original sign in the physical world, and perform an evaluation using the image captured by a car dash camera from the same distance. Table 2 shows the results. As seen in the first and second columns of this table, FragGAN is able to generate adversarial fragments that are visually indistinguishable from the original ones, thus satisfying the clean-label property. The last column of Table 2 demonstrate that FragGAN is able to mislead the steering angle by a noticeable degree, specifically, 13.2 and 19.8 degrees for the McDonald’s and Apple Watch scene, respectively.

		Physical Test	
		Fragments	Scene
Mc			
Apple			

Table 2: Physical-world case studies using FragGAN, which generates adversarial fragments (first column) corresponding to the original roadside advertising signs (second column). The third column shows the snapshot of the physical world case study where the fragments are printed out and pasted onto the original sign, where the blue (red) arrow indicates the ground truth (erroneous) steering angle.

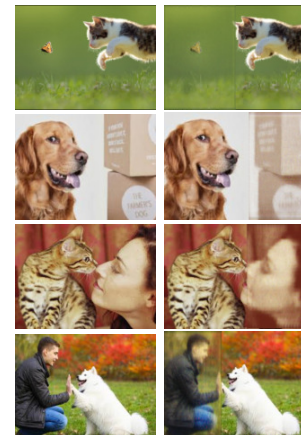


Figure 5: Original samples (left subfigure of each row) and the generated adversarial samples (right subfigure of each row).

	FGSM	AdvGAN	AdvGAN(Frag)	FragGAN
Dog	6.2%	13.3%	9.7%	11.5%
Cat	5.8%	12.5%	7.6%	8.7%
Bridge	7.3%	11.7%	5.5%	12.2%
Tower	8.6%	12.9%	6.1%	11.7%

Table 3: Comparison results.

4.2 Applying FragGAN to Image Classification

We also evaluate the effectiveness of applying FragGAN to attack image classification models on two different datasets. We first trained a dog-cat classification neural network using the dataset "Dogs vs. Cats kag (2019)" as the target model. We selected another 217 images (113 dog images and 104 cat images) as the test samples. We also trained a classification neural network using LSUN Yu et al. (2015), and the test set consists of 326 images (163 tower images and 163 bridge images). Note that we perform this set of the experiment using a limited set of dataset due to the fact that for each image in the evaluated dataset, we have to mark the 4 coordinates of the fragments targeted by FragGAN. The goal is to use FragGAN to generate adversarial fragments with attacking effectiveness without modifying pixels belonging to the essential content of each image (i.e., dog or cat). We compare against existing methods, including FGSM, AdvGAN, and AdvGAN(fragment).

Fig. 5 shows several samples of the original images and the generated images with the adversarial fragments. We observe that FragGAN is able to generate fragments which are visually indistinguishable from the original, without even touching any area that contains the essential content. Table 3 shows the attack success rate on the dataset. As seen in the table, only AdvGAN yields better performance than FragGAN due to the unfair comparison, where FragGAN only modifies a non-essential fragment while AdvGAN is allowed to add perturbations to the entire image. When given a fair comparison, i.e., against AdvGAN(Frag), we observe a clearly superior performance yielded by FragGAN for both sets of experiments. FragGAN is able to increases the attacking success rate by 1.8% and 6.7% for the "Dog vs. Cat" and the "bridge and tower" LSUN dataset, respectively. This proves the attacking effectiveness of FragGAN which does not need to modify any essential content of the input.

5 Conclusion

In this paper, we propose FragGAN, a GAN-based framework that is capable of generating effective and arbitrary adversarial quadrilateral fragments within any input image. FragGAN enables effective and clean-label attacks applicable to (and implementable under) physical world scenarios such as autonomous driving. Experimental results on both autonomous steering and image classification models prove that FragGAN is highly effective and superior to state-of-the-art approaches.

References

- (2019). "<https://www.geometrictools.com/Documentation/PerspectiveMappings.pdf>".
- (2019). "<https://en.wikipedia.org/wiki/Interpolation>".
- (2019a). "<https://devblogs.nvidia.com/deep-learning-self-driving-cars/>".
- (2019). "<https://medium.com/udacity/challenge-2-using-deep-learning-to-predict-steering-angles-f42004a36ff3>".
- (2019b). "<https://github.com/SullyChen/driving-datasets>".
- (2019). "<https://www.kaggle.com/c/dogs-vs-cats/data>".
- Athalye, A., Engstrom, L., Ilyas, A., and Kwok, K. (2017). Synthesizing robust adversarial examples. *arXiv preprint arXiv:1707.07397*.
- Carlini, N. and Wagner, D. (2017). Towards evaluating the robustness of neural networks. In *2017 IEEE Symposium on Security and Privacy (SP)*, pages 39–57. IEEE.
- Elsayed, G., Shankar, S., Cheung, B., Papernot, N., Kurakin, A., Goodfellow, I., and Sohl-Dickstein, J. (2018). Adversarial examples that fool both computer vision and time-limited humans. In *Advances in Neural Information Processing Systems*, pages 3914–3924.

Eykholt, K., Evtimov, I., Fernandes, E., Li, B., Rahmati, A., Xiao, C., Prakash, A., Kohno, T., and Song, D. (2017). Robust physical-world attacks on deep learning models. *arXiv preprint arXiv:1707.08945*.

Eykholt, K., Evtimov, I., Fernandes, E., Li, B., Rahmati, A., Xiao, C., Prakash, A., Kohno, T., and Song, D. (2018a). Robust physical-world attacks on deep learning visual classification. In *Proceedings of the IEEE Conference on Computer Vision and Pattern Recognition*, pages 1625–1634.

Eykholt, K., Evtimov, I., Fernandes, E., Li, B., Rahmati, A., Xiao, C., Prakash, A., Kohno, T., and Song, D. (2018b). Robust physical-world attacks on deep learning visual classification. In *CVPR*, pages 1625–1634.

Geiger, A., Lenz, P., Stiller, C., and Urtasun, R. (2013). Vision meets robotics: The kitti dataset. *The International Journal of Robotics Research*, 32(11):1231–1237.

Goodfellow, I., Pouget-Abadie, J., Mirza, M., Xu, B., Warde-Farley, D., Ozair, S., Courville, A., and Bengio, Y. (2014a). Generative adversarial nets. In *Advances in neural information processing systems*, pages 2672–2680.

Goodfellow, I. J., Shlens, J., and Szegedy, C. (2014b). Explaining and harnessing adversarial examples. *arXiv preprint arXiv:1412.6572*.

He, K., Gkioxari, G., Dollár, P., and Girshick, R. (2017). Mask r-cnn. In *Proceedings of the IEEE international conference on computer vision*, pages 2961–2969.

Hinton, G., Deng, L., Yu, D., Dahl, G., Mohamed, A.-r., Jaitly, N., Senior, A., Vanhoucke, V., Nguyen, P., Kingsbury, B., et al. (2012). Deep neural networks for acoustic modeling in speech recognition. *IEEE Signal processing magazine*, 29.

Hinton, G., Vinyals, O., and Dean, J. (2015). Distilling the knowledge in a neural network. *arXiv preprint arXiv:1503.02531*.

Hu, W. and Tan, Y. (2017). Generating adversarial malware examples for black-box attacks based on gan. *arXiv preprint arXiv:1702.05983*.

Isola, P., Zhu, J.-Y., Zhou, T., and Efros, A. A. (2017). Image-to-image translation with conditional adversarial networks. In *CVPR*, pages 1125–1134.

Karmon, D., Zoran, D., and Goldberg, Y. (2018). Lavan: Localized and visible adversarial noise. *arXiv preprint arXiv:1801.02608*.

Kos, J., Fischer, I., and Song, D. (2018). Adversarial examples for generative models. In *2018 IEEE Security and Privacy Workshops (SPW)*, pages 36–42. IEEE.

Kurakin, A., Goodfellow, I., and Bengio, S. (2016). Adversarial machine learning at scale. *arXiv preprint arXiv:1611.01236*.

Li, B. and Vorobeychik, Y. (2014). Feature cross-substitution in adversarial classification. In *Advances in neural information processing systems*, pages 2087–2095.

Li, B. and Vorobeychik, Y. (2015). Scalable optimization of randomized operational decisions in adversarial classification settings. In *Artificial Intelligence and Statistics*, pages 599–607.

Lin, Y.-C., Hong, Z.-W., Liao, Y.-H., Shih, M.-L., Liu, M.-Y., and Sun, M. (2017). Tactics of adversarial attack on deep reinforcement learning agents. *arXiv preprint arXiv:1703.06748*.

Liu, Y., Chen, X., Liu, C., and Song, D. (2016). Delving into transferable adversarial examples and black-box attacks. *arXiv preprint arXiv:1611.02770*.

Lu, Y., Tai, Y.-W., and Tang, C.-K. (2017). Conditional cyclegan for attribute guided face image generation. *arXiv preprint arXiv:1705.09966*.

Ma, L., Juefei-Xu, F., Zhang, F., Sun, J., Xue, M., Li, B., Chen, C., Su, T., Li, L., Liu, Y., et al. (2018). Deepgauge: Multi-granularity testing criteria for deep learning systems. In *Proceedings of the 33rd ACM/IEEE International Conference on Automated Software Engineering*, pages 120–131. ACM.

Metzen, J. H., Kumar, M. C., Brox, T., and Fischer, V. (2017). Universal adversarial perturbations against semantic image segmentation. In *2017 IEEE International Conference on Computer Vision (ICCV)*, pages 2774–2783. IEEE.

Mogelmose, A., Trivedi, M. M., and Moeslund, T. B. (2012). Vision-based traffic sign detection and analysis for intelligent driver assistance systems: Perspectives and survey. *IEEE Transactions on Intelligent Transportation Systems*, 13(4):1484–1497.

Moosavi-Dezfooli, S.-M., Fawzi, A., and Frossard, P. (2016). Deepfool: a simple and accurate method to fool deep neural networks. In *Proceedings of the IEEE conference on computer vision and pattern recognition*, pages 2574–2582.

Pan, X., You, Y., Wang, Z., and Lu, C. (2017). Virtual to real reinforcement learning for autonomous driving. *arXiv preprint arXiv:1704.03952*.

Pei, K., Cao, Y., Yang, J., and Jana, S. (2017). Deepxplore: Automated whitebox testing of deep learning systems. In *proceedings of the 26th Symposium on Operating Systems Principles*, pages 1–18. ACM.

Sermanet, P. and LeCun, Y. (2011). Traffic sign recognition with multi-scale convolutional networks. In *IJCNN*, pages 2809–2813.

Sharif, M., Bhagavatula, S., Bauer, L., and Reiter, M. K. (2016). Accessorize to a crime: Real and stealthy attacks on state-of-the-art face recognition. In *Proceedings of the 2016 ACM SIGSAC Conference on Computer and Communications Security*, pages 1528–1540. ACM.

Song, Y., Shu, R., Kushman, N., and Ermon, S. (2018). Constructing unrestricted adversarial examples with generative models. In *Advances in Neural Information Processing Systems*, pages 8312–8323.

Szegedy, C., Zaremba, W., Sutskever, I., Bruna, J., Erhan, D., Goodfellow, I., and Fergus, R. (2013). Intriguing properties of neural networks. *arXiv preprint arXiv:1312.6199*.

Tanay, T. and Griffin, L. (2016). A boundary tilting persepective on the phenomenon of adversarial examples. *arXiv preprint arXiv:1608.07690*.

Tian, Y., Pei, K., Jana, S., and Ray, B. (2018). Deeptest: Automated testing of deep-neural-network-driven autonomous cars. In *Proceedings of the 40th international conference on software engineering*, pages 303–314. ACM.

Xiao, C., Li, B., Zhu, J.-Y., He, W., Liu, M., and Song, D. (2018a). Generating adversarial examples with adversarial networks. *arXiv preprint arXiv:1801.02610*.

Xiao, C., Zhu, J.-Y., Li, B., He, W., Liu, M., and Song, D. (2018b). Spatially transformed adversarial examples. *arXiv preprint arXiv:1801.02612*.

Yu, F., Seff, A., Zhang, Y., Song, S., Funkhouser, T., and Xiao, J. (2015). Lsun: Construction of a large-scale image dataset using deep learning with humans in the loop. *arXiv preprint arXiv:1506.03365*.

Zhang, M., Zhang, Y., Zhang, L., Liu, C., and Khurshid, S. (2018). Deeproad: Gan-based metamorphic autonomous driving system testing. *arXiv preprint arXiv:1802.02295*.

Zhou, H., Li, W., Zhu, Y., Zhang, Y., Yu, B., Zhang, L., and Liu, C. (2018). Deepbillboard: Systematic physical-world testing of autonomous driving systems. *arXiv preprint arXiv:1812.10812*.

Zhu, J.-Y., Krähenbühl, P., Shechtman, E., and Efros, A. A. (2016). Generative visual manipulation on the natural image manifold. In *ECCV*, pages 597–613. Springer.

Zhu, J.-Y., Park, T., Isola, P., and Efros, A. A. (2017). Unpaired image-to-image translation using cycle-consistent adversarial networks. In *ICCV*, pages 2223–2232.

Appendix (as Supplementary Material)

Detailed description on the attributes of the selected scenes (Sec. 4.1).

The evaluated eight scenes in each dataset cover both straight and curved lane scenarios. Since all these datasets do not contain coordinates of roadside signs, we have to label the four corners of the signs in every frame of the selected scenes. We use the motion tracker functionality of Adobe After Effects¹ to automatically track the movement of the sign's four corners among consecutive frames. Table 4 shows the attributes of the scenes we selected. Table 5 shows a sample original targeted fragment and the corresponding image frame under the eight evaluated scenes.

Scenes	Images	Size	min	max
Dave-straight1	54	455 × 256	21 × 22	41 × 49
Dave-curve1	34	455 × 256	29 × 32	51 × 49
Udacity-straight1	22	640 × 480	48 × 29	66 × 35
Udacity-curve1 (1)(2)	80	640 × 480	51 × 51	155 × 156
Kitti-straight1	20	455 × 1392	56 × 74	121 × 162
Kitti-straight2	21	455 × 1392	80 × 46	247 × 100
Kitti-curve1	21	455 × 1392	64 × 74	173 × 223

Table 4: Scenes evaluated in the experiments.

	Dave		Udacity			Kitti		
	Straight1	Curve1	Straight1	Curve1(1)	Curve1(2)	Straight1	Curve1	Straight2
Original								

Table 5: The original targeted fragments and the corresponding entire image frames under various scenes. Note that Tables 6-9 generate adversarial fragments under different models corresponding to the original scenes presented in this table.

¹<https://www.adobe.com/products/aftereffects.html>

Additional Evaluation Results on All Evaluated Four Autonomous Steering Models, Three Datasets, and Eight Scenes

In our submitted draft, due to space constraints, we only present evaluation results using the DAVE-2 steering model and a partial set of datasets and scenes. We now present all the evaluation results using all four state-of-the-art steering models including Dave-2, Dave-2_V2,² Dave-2_V3,³ and the Epoch model from the Udacity challenge.⁴ Dave-2 is the original CNN architecture presented in NVIDIA’s Dave-2 System (Fig 6). Dave-2_V2 is a variation of Dave-2 which normalizes the randomly initialized net work weights and removes the first batch normalization layer. Dave-2_V3 is another publicly available steering model which modifies the original Dave model by removing two convolution layers and one fully connected layer, and inserting two dropout layers among the three fully connected layers. As a pre-trained model, Epoch’s weights are not publicly available, we train it following the instructions provided by the corresponding authors using the Udacity self-driving Challenge dataset.⁵

Tables 6–9 respectively show a demonstration of the adversarial examples generated by FragGAN based upon the original image frames shown in Table 5 for the aforementioned four steering models. For each scene, the blue arrows indicate ground truth steering angles, the red arrows indicate steering angle due to the adversarial sample generated by FragGAN under original steering models, and the green arrows indicate steering angle affected by the adversarial sample generated by FragGAN under the corresponding distilled model. As we can observe from table, FragGAN is able to generate rather realistic adversarial fragments (thus images) which are visually indistinguishable from the original ones.

Fig. 7–10 show the attacking effectiveness results on the four evaluated autonomous steering models in terms of the steering angle error along the timeline for all eight scenes. The results are similar to Fig. 3 presented in the submitted draft, which prove FragGAN to be effective and robust in attacking various state-of-the-art steering models and datasets.

²<https://github.com/jacobgil/keras-steering-angle-visualizations>

³<https://github.com/navoshta/behavioral-cloning>

⁴<https://github.com/udacity/self-driving-car/tree/master/steering-models/community-models/cg23>

⁵<https://medium.com/udacity/challenge-2-using-deep-learning-to-predict-steering-angles-f42004a36ff3>

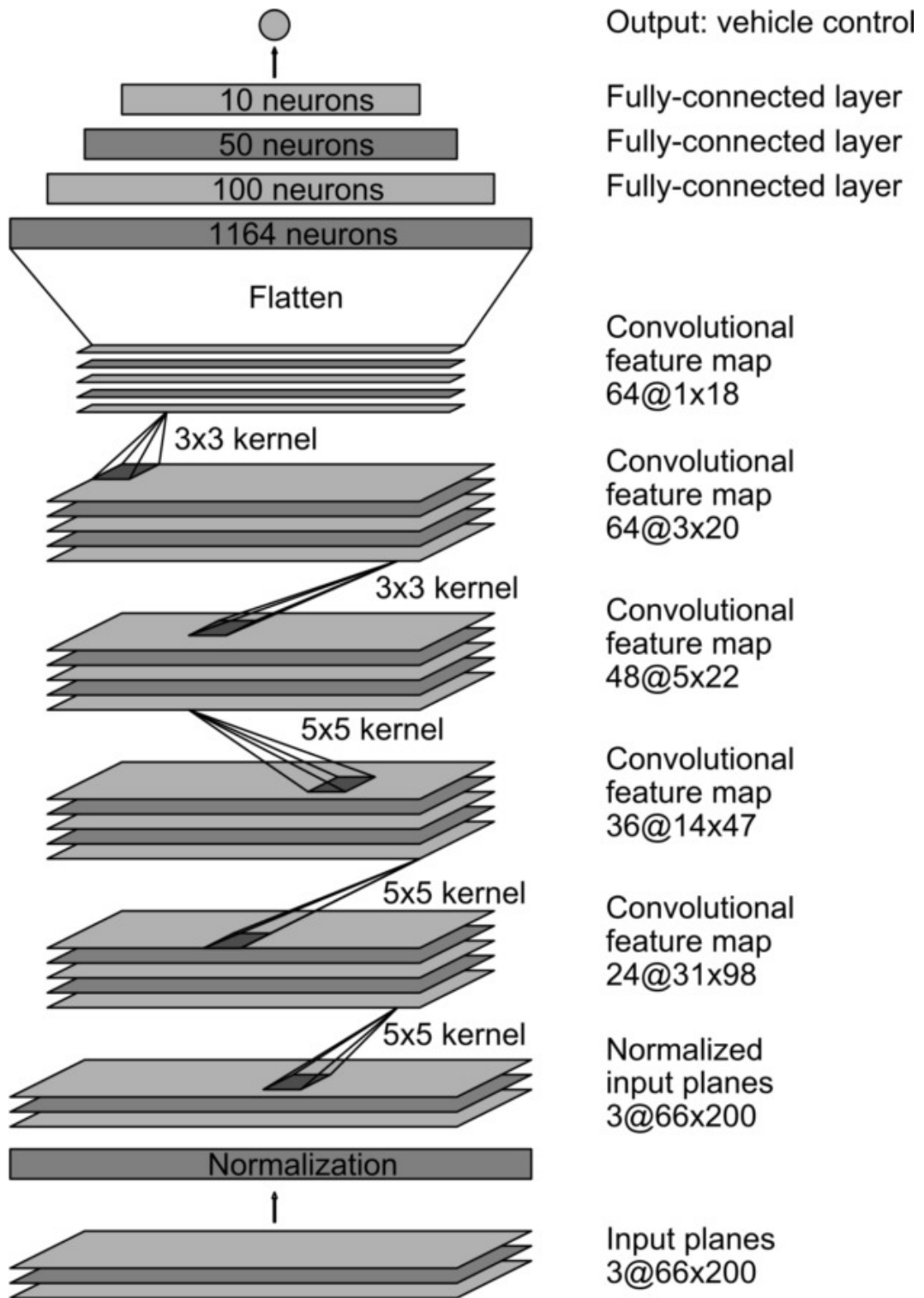


Figure 6: Architecture of Dave-2.

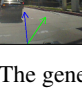
	Dave		Udacity			Kitti		
	Straight1	Curve1	Straight1	Curve1(1)	Curve1(2)	Straight1	Curve1	Straight2
Distilled DAVE-2								
Distilled DAVE-2								

Table 6: The generated adversarial fragments under Dave-2 and its distilled model.

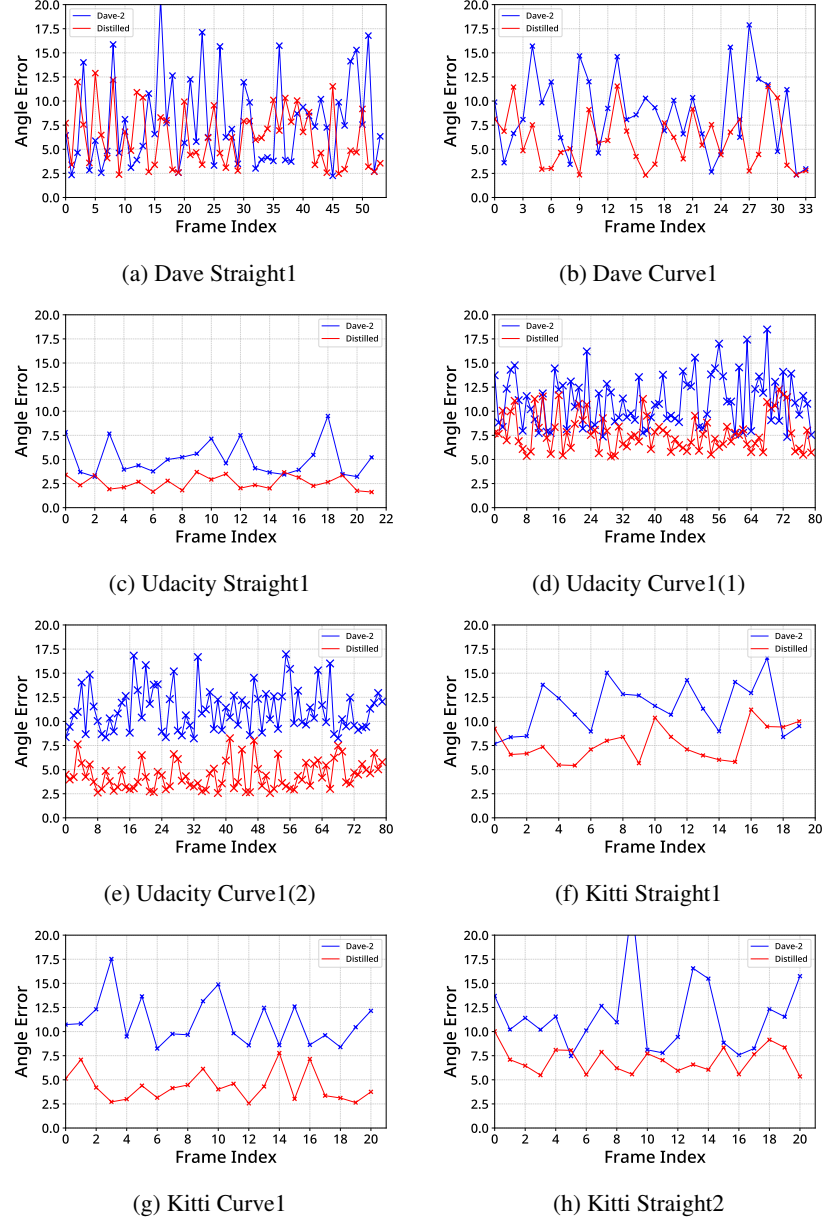


Figure 7: Results on the steering angle error under Dave-2.

	Dave		Udacity		Kitti			
	Straight1	Curve1	Straight1	Curve1(1)	Curve1(2)	Straight1	Curve1	Straight2
DAVE-2 V2								
Distilled								

Table 7: The generated adversarial fragments under Dave-2_V2 and its distilled model.

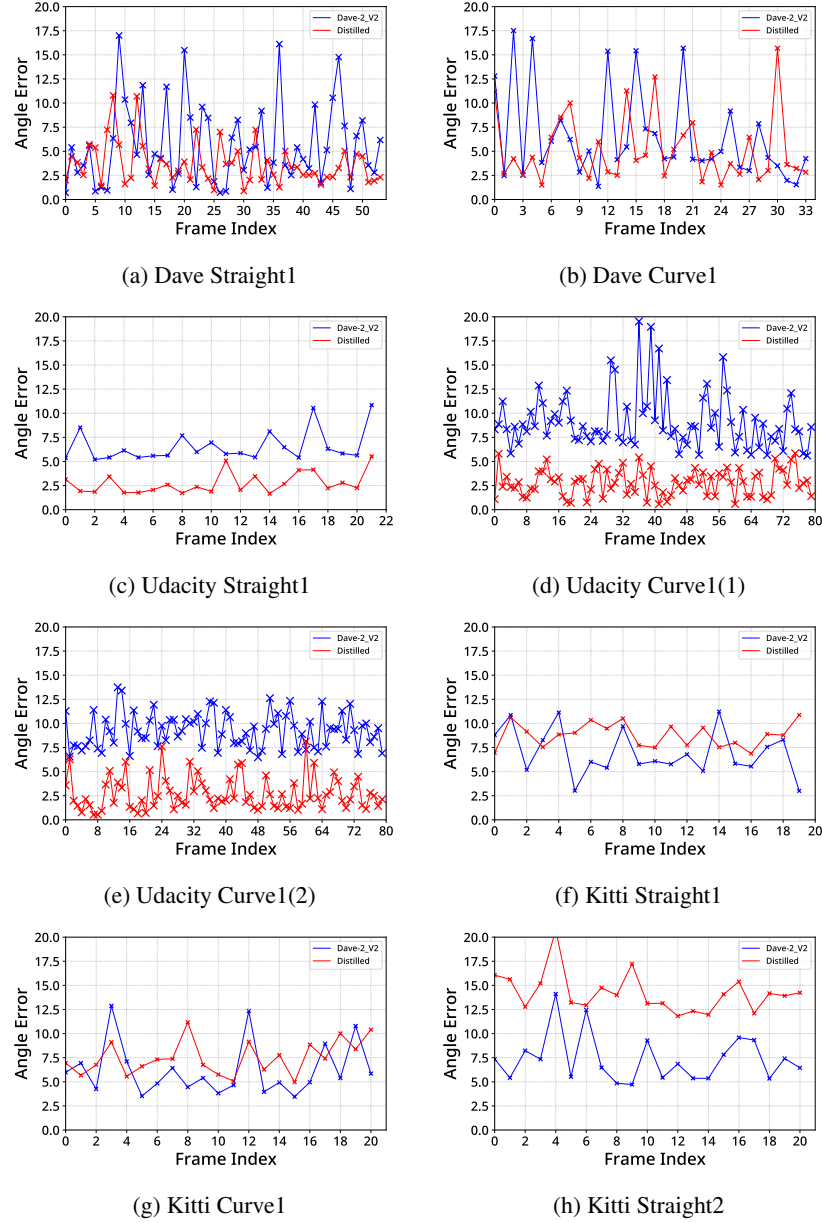


Figure 8: Results on the steering angle error under Dave-2_V2.

	Dave		Udacity		Kitti			
	Straight1	Curve1	Straight1	Curve1(1)	Curve1(2)	Straight1	Curve1	Straight2
DAVE-2 V3								
Distilled								

Table 8: The generated adversarial fragments under Dave-2_V3 and its distilled model.

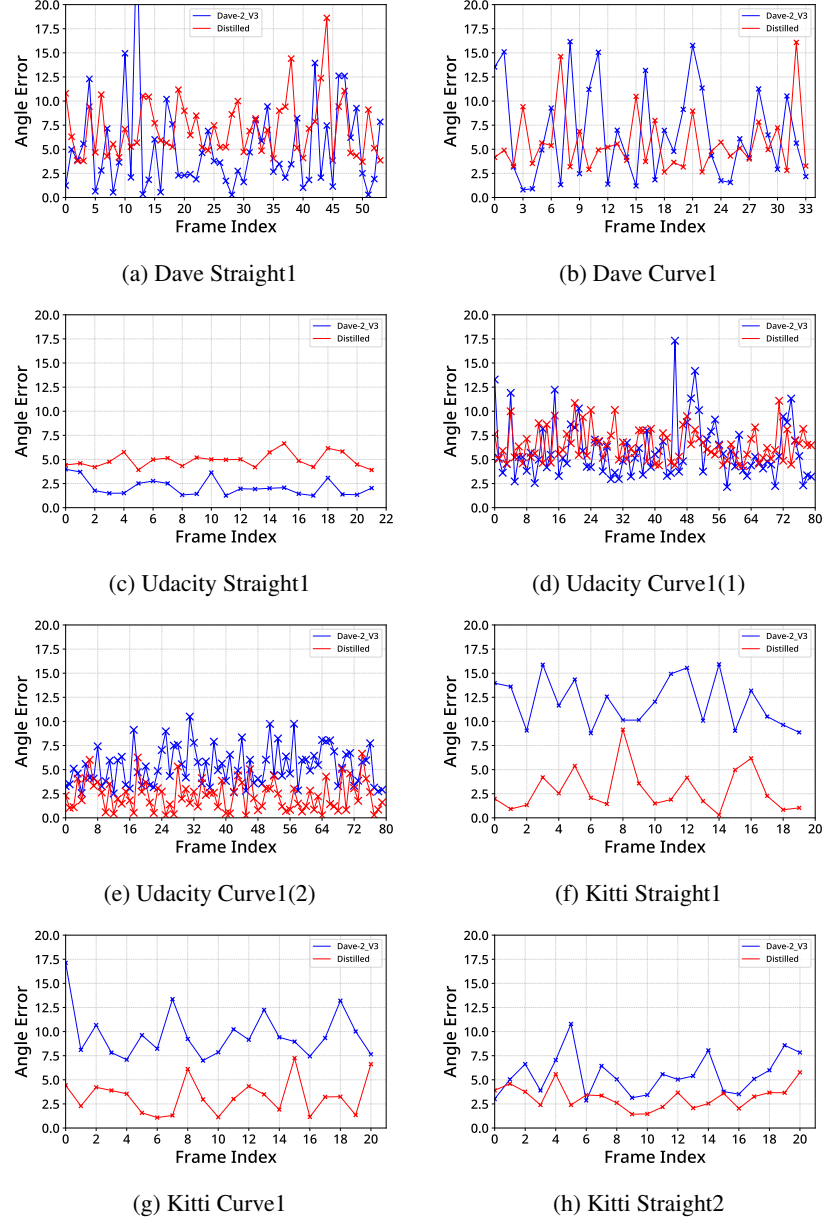


Figure 9: Results on the steering angle error under Dave-2_V3

	Dave		Udacity			Kitti		
	Straight1	Curve1	Straight1	Curve1(1)	Curve1(2)	Straight1	Curve1	Straight2
Epoch								
Distilled								

Table 9: The generated adversarial fragments under Epoch and its distilled model.

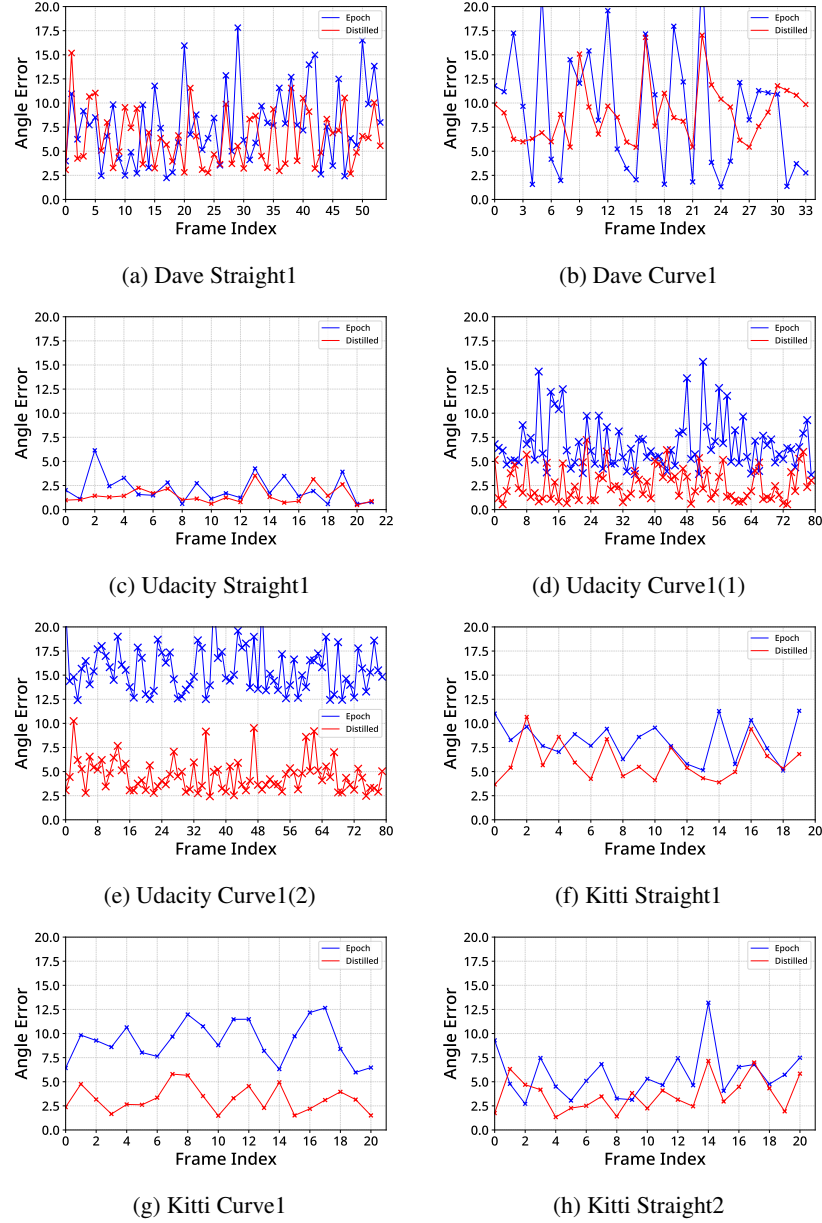


Figure 10: Results on the steering angle error under Epoch